J. Phys. B: At. Mol. Opt. Phys. 24 (1991) 963–975. Printed in the UK

# H($n = 2$ and 3) density matrices produced in proton–helium collisions at intermediate energies

R Shingal and C D Lin

Physics Department, Cardwell Hall, Kansas State University, KS 66506-2604, USA

Received 14 August 1990, in final form 19 November 1990

**Abstract.** Density matrices for the excited H($n = 2$ and 3) atoms produced in the electron transfer collisions between protons and helium atoms have been calculated for impact energies between 15 and 100 keV. The multichannel semiclassical impact parameter model with straight-line trajectories and an expansion in travelling atomic orbitals was used. The helium atom was approximated by a single electron moving in an effective potential. The calculated density matrices, the electric dipole moment and the first moment of the electron current density distribution are compared with recent experimental data of Ashburn *et al.*

## 1. Introduction

The excited states of hydrogen atoms formed by the electron capture process in collisions of protons and helium atoms are coherently excited. The coherence, which can be formally represented by the off-diagonal elements of the density matrix or in terms of state multipoles, can be experimentally determined by detecting the polarization and the angular distribution of the emitted photon in an external electric field (Krotkov 1975, Eck 1973). Partial information of the coherence can also be obtained by observing the quantum beats (Sellin *et al* 1973, DeSerio *et al* 1988). In a series of recent papers, Jain *et al* (1987a, b, 1988) calculated and analysed the density matrices of the excited H($n = 2$ and 3) states for p-He collisions at intermediate projectile velocities ($v = 1$–$2$ au). By adopting a model potential to describe the helium atom, these authors solved the pseudo-one-electron collision problem using the semiclassical impact parameter formulation where the time-dependent total electronic wavefunction was expanded in terms of the travelling atomic orbitals placed on both centres. The density matrices, as well as state multipoles, constructed from the calculated scattering amplitudes were then compared with those derived previously from experiments (Brower and Pipkin 1986, Havener *et al* 1986). The predicted density matrices and the state multipoles were found to be in qualitative agreement with the available experimental data.

Recent improved measurements (after a careful determination of electric fields in the collision region) for the same collision system have revealed quantitative discrepancies between these earlier calculations and the experimental data (Ashburn *et al* 1990). From the theoretical point of view, the discrepancy can be attributed to two major assumptions adopted in these earlier calculations. (i) The use of the one-electron model for the actual two-electron collision system. This model was 'justified' for the fast collisions under study in that the passive electron does not affect the active electron during the short period of time in which the transition takes place. (ii) The limitation

0953-4075/91/050963+13$03.50  

of the size of the basis set used. In the 25–100 keV energy region, cross sections for single ionization of the helium atom are quite large. In the presence of these large channels, one is then interested in the elements of the density matrices for the small channels of electron capture to the excited $n = 2$ and $n = 3$ manifolds of the hydrogen atoms. Jain *et al* used a 19-state basis set comprising the ground state of the helium atom, the $n = 1$, 2 and 3 states on the hydrogen atom and a few pseudostates to represent the ionization channels.

In this paper, the density matrices and the H($n = 2$) and H($n = 3$) states formed in proton–helium collisions over the 25–100 keV energy region have been re-examined using the same one-electron model but with a considerably enlarged basis set. The excitation channels neglected in the earlier calculation of Jain *et al* (1987a) along with a more complete representation of the ionization channels have been included. While computer codes for carrying out the full two-electron close-coupling calculations using a two-centre atomic orbital expansion method do exist (Bransden *et al* 1984, Fritsch and Lin 1986, Shingal and Bransden 1989, Shingal *et al* 1989), all the existing calculations have been limited to relatively small basis sets.

A brief overview of the theoretical method, the definition of several state multipoles and the basis functions used in the calculation are given in section 2. The calculated elements of the density matrix and the coherent parameters are compared with experimental data in section 3. Finally, some conclusions are drawn in section 4.

## 2. Theoretical methods and state multipoles

A detailed treatment of the theoretical method pertaining to the present investigation has been given in Jain *et al* (1987a, b). The major differences and the relevant sections are outlined here.

The two-electron proton–helium collision system was reduced to a quasi-one-electron system where the active electron of the helium atom experienced an effective potential presented by the helium nucleus and the passive electron. The effective potential takes the form

$$V_{\text{eff}}(r) = -z_1/r - (z_2 + z_3 r)\, \mathrm{e}^{-\alpha r}/r \tag{1}$$

where $z_1 = z_2 = 1.0$, $z_3 = 0.4143$ and $\alpha = 2.499$.

The time-dependent Schrödinger equation

$$(H_{\text{el}} - \mathrm{i}\partial/\partial t)\Psi = 0 \tag{2}$$

was solved in the impact parameter formalism. The total wavefunction, $\Psi$, of the combined system was expanded in atomic orbitals placed on their respective centres:

$$\Psi = \sum_i a_i \phi_i(\boldsymbol{r}_{\text{T}}) + \sum_j a_j \phi_j(\boldsymbol{r}_{\text{P}}). \tag{3}$$

The atomic orbitals for the asymptotic hydrogen and the helium atoms were generated by diagonalizing the respective Hamiltonian on a basis set consisting of Slater orbitals ($r^{p_i} \exp(-\lambda_i r)$) for each angular momentum state. A basis set consisting of 64 states comprising 6 s-type, 6 p-type and 6 d-type states on the helium target and 8 s-type, 7 p-type and 4 d-type states on the projectile was used. The energies and the constants $p_i$ and $\lambda_i$ for the Slater-type orbitals placed on the target and the projectile centre are given in tables 1 and 2, respectively. We note that the present basis set is not capable of reproducing the binary encounter peak in ionizing collisions due to the limitation

**Table 1.** Eigenenergies and parameters of the Slater-type orbitals used to construct helium eignstates.

| $l$ | $p_i$ | $\lambda_i$ | Eigenenergies (au) |
|---|---|---|---|
| 0 | 0 | 1.6655 | −0.903 |
| | 0 | 0.9425 | −0.155 |
| | 0 | 0.1531 | −0.064 |
| | 2 | 1.1425 | −0.033 |
| | 2 | 0.2814 | 0.082 |
| | 3 | 0.5146 | 1.471 |
| 1 | 1 | 1.6655 | −0.128 |
| | 1 | 0.3995 | −0.057 |
| | 1 | 0.1631 | −0.032 |
| | 2 | 1.3995 | 0.011 |
| | 2 | 0.3631 | 0.308 |
| | 3 | 0.5631 | 1.979 |
| 2 | 2 | 1.6655 | −0.055 |
| | 2 | 0.3935 | −0.026 |
| | 2 | 0.2631 | 0.241 |
| | 3 | 1.3995 | 1.647 |

**Table 2.** Eigenenergies and parameters of the Slater-type orbitals used to construct hydrogen eigenstates.

| $l$ | $p_i$ | $\lambda_i$ | Eigenenergies (au) |
|---|---|---|---|
| 0 | 0 | 1.0000 | −0.500 |
| | 0 | 0.5000 | −0.125 |
| | 0 | 0.3333 | −0.055 |
| | 1 | 0.5000 | −0.030 |
| | 1 | 0.3333 | 0.007 |
| | 2 | 0.3333 | 0.123 |
| | 2 | 0.8000 | 0.511 |
| | 3 | 1.4000 | 2.875 |
| 1 | 1 | 1.0000 | −0.125 |
| | 1 | 0.5000 | −0.055 |
| | 1 | 0.3333 | −0.031 |
| | 1 | 0.2000 | −0.014 |
| | 2 | 0.3333 | 0.065 |
| | 2 | 0.8000 | 0.312 |
| | 3 | 1.4000 | 1.363 |
| 2 | 2 | 0.3333 | −0.055 |
| | 2 | 1.1000 | −0.019 |
| | 3 | 0.6000 | 0.096 |
| | 3 | 0.8000 | 0.670 |

on the maximum positive energy allowed for the outgoing electron. However, the total ionization cross section is not sensitive to these high energy electrons. Furthermore, the present results were found to be insensitive to increasing the basis set to 72 states for test calculations. The plane-wave translational factors were included and the heavy nuclei were assumed to follow a rectilinear trajectory. The scattering amplitudes, $a_{nlm}$, for the excitation of a particular *nlm* state of the hydrogen atom were obtained by solving a set of first-order coupled differential equations for each impact parameter (see, for example, Shingal 1988).

The passage of protons through a gas of helium atoms results in coherently excited hydrogen atoms for a given degenerate manifold. These can be described by a pure state

$$\Psi = \sum_i a_{nlm}(b, t=\infty)\Phi_{nlm}(\boldsymbol{r}). \tag{4}$$

The integrated (over impact parameters) density matrix elements can be written in terms of the scattering amplitudes

$$\bar{\rho}_{nlm,n'l'm'} = \int_0^{2\pi}\int_0^{\infty} a_{nlm}(b)a^*_{n'l'm'}(b)b\ \mathrm{d}b. \tag{5}$$

Here *lm* corresponds to a particular level. It is noted that the symmetry consideration limits the number of independent elements. Furthermore, the density matrix contains all the information regarding the collision events.

The diagonal elements of the density matrix are related to the cross section for excitation of the particular state *nlm*. Direct interpretations of the off-diagonal elements are more difficult. Instead of the density matrix itself, one can define state multipoles which have classical interpretations (Blum 1981, Fano and Macek 1973). For the coherence within a degenerate excited hydrogenic manifold, one of the state multipoles (Burgdorfer 1983) which has the simple physical interpretation is the $z$ component of the dipole moment (or the first moment of the charge density). The average dipole moment $\langle D_z\rangle$ for the $n=2$ and $n=3$ manifold of the hydrogen atom is given by

$$\langle D_z\rangle_{n=2} = 6\ \mathrm{Re}(\bar{\rho}_{00,10})/\mathrm{Tr}(\bar{\rho}_{n=2}) \tag{6}$$

and

$$\langle D_z\rangle_{n=3} = 6\sqrt{6}\ \mathrm{Re}(\bar{\rho}_{00,10}+\sqrt{\tfrac{1}{2}}\,\bar{\rho}_{10,20}+\sqrt{\tfrac{3}{2}}\,\bar{\rho}_{11,21})/\mathrm{Tr}(\bar{\rho}_{n=3}). \tag{7}$$

It is noted that the sign of the dipole moment can be related with the position of the electron with respect to the nucleus, namely a positive value implies that the captured electron lags behind the proton.

The imaginary parts of the off-diagonal matrix elements can be related to the expectation values of $\boldsymbol{L}\times\boldsymbol{A}$ constructed from the angular momentum vector $\boldsymbol{L}$ and the Runge–Lenz vector $\boldsymbol{A}$. Classically this vector is proportional to the velocity of the electron at the perihelion of the Kepler orbit. The average $z$ component of the symmetrized combination of the vector $\boldsymbol{L}\times\boldsymbol{A}$ is

$$\langle(\boldsymbol{L}\times\boldsymbol{A})_{z,s}\rangle = -2\ \mathrm{Im}(\bar{\rho}_{00,10})/\mathrm{Tr}(\bar{\rho}_{n=2}) \tag{8}$$

and

$$\langle(\boldsymbol{L}\times\boldsymbol{A})_{z,s}\rangle = 4\sqrt{\tfrac{2}{3}}\ \mathrm{Im}(\bar{\rho}_{00,10}+\sqrt{2}\bar{\rho}_{10,20}+\sqrt{6}\,\bar{\rho}_{11,21})/\mathrm{Tr}(\bar{\rho}_{n=3}) \tag{9}$$

for the $n=2$ and $n=3$ degenerate manifold of the hydrogen atom, respectively.

For integral measurements where the scattering angles of the projectiles are not determined, another coherence parameter that can be determined is the alignment

parameter, $A_{20}$. For p states, it can be expressed in terms of the $\sigma_0$ and $\sigma_1$ partial cross sections for $H(2p_0)$ and $H(2p_1)$ excitation, respectively as

$$A_{20}=\frac{\sigma_1-\sigma_0}{\sigma_0+2\sigma_1}. \tag{10}$$

In this paper, in addition to partial electron capture cross sections to individual excited states, we obtain the density matrix, the dipole moment, the first-order moment of the current density and the alignment parameter calculated from the present calculation. These results, obtained in a single calculation, are compared with existing experiments.

## 3. Results and discussions

The calculated partial $(nl)$ and total cross sections for the production of hydrogen atoms in collisions of protons with helium atoms do not differ significantly from the early results of Jain *et al* (1987a, b), and are in good agreement with the available experimental data. For brevity, these calculated cross sections are not reported here. The results of theoretical calculations of Jain *et al* (1987a, b) have been compared with the experimental data by Ashburn *et al* (1990). These are also not displayed in the present work.

### *3.1. Dipole moment and the first moment of the electron current density*

The calculated averaged dipole moment $\langle D_z\rangle$ and the averaged velocity vector $\langle(\boldsymbol{L}\times\boldsymbol{A})_z\rangle$ for the excited $n=2$ hydrogen atom are displayed in figures 1($a$) and ($b$). From (6), $\langle D_z\rangle$ measures the real part of the off-diagonal density matrix element between 2s and $2p_0$. The calculated dipole moment is positive in the entire energy region under consideration, indicating that the captured electron always falls behind the projectile

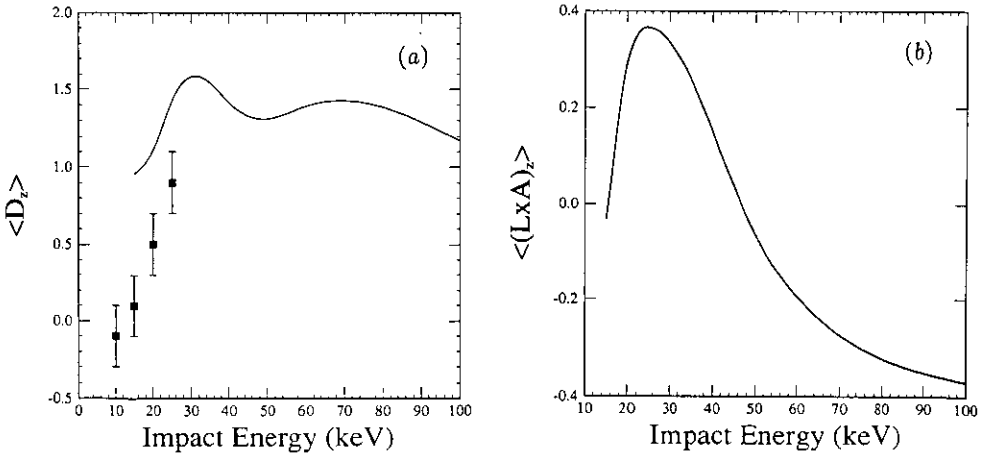


**Figure 1.** ($a$) electric dipole moment $\langle D_z\rangle$ for $H^+ + He(1s^2) \rightarrow H(n=2) + He^+$. Theory: ——, present results. Experiment: ■, Hippler (1990). ($b$) Present theoretical results for $\langle(\boldsymbol{L}\times\boldsymbol{A})_z\rangle$.

centre in the collision. The dipole moment attains a value of 1.54 au at 35 keV, which is to be compared with the maximum allowed value of 3.0 au for H($n=2$). (The maximum dipole moment is achieved when the excited hydrogen atom is placed in a static electric field.) In figure 1($a$), the measured low energy dipole moment (Hippler 1990) is also shown. Although the calculation does indicate decreasing dipole moments with decreasing energies, in agreement with the experimental data, the theoretical calculations below 30–40 keV should not be taken too seriously since the applicability of the one-electron model at such low energies is questionable. Furthermore, a significant influence of the two-electron processes cannot be excluded for the entire energy range studied in the present work. The calculated expectation value of the velocity vector $(\boldsymbol{L}\times\boldsymbol{A})_z$, as shown in figure 1($b$), is positive for impact energies below 50 keV and remains negative for higher energies. The lack of experimental data for this quantity for H($n=2$) capture is noted.

The present calculated values of $\langle D_z\rangle$ and $\langle(\boldsymbol{L}\times\boldsymbol{A})_z\rangle$ for H($n=3$) states are compared with the recent measured values of Ashburn *et al* (1990) in figures 2($a$) and ($b$). The comparison between earlier theoretical results of Jain *et al* (1987a, b) and the experimental data has already been shown by Ashburn *et al* (1990). The dipole moment is again positive throughout the energy region considered indicating that the captured electron lags behind the proton. In contrast to the maximum theoretically ascribed value of 7.5 au for the H($n=3$) states, the maximum calculated dipole moment is 5.14 au. The calculated dipole moment is in qualitative agreement with the experimental data. Quantitatively, it overestimates the measured values, especially at higher energies. In contrast, a good agreement between the calculated and the measured values of the velocity vector $\langle(\boldsymbol{L}\times\boldsymbol{A})_z\rangle$ is found.

### *3.2. Cross sections for capture to individual nlm states*

The full density matrix for H($n=3$), normalized with respect to the diagonal 3s term, has been deduced by the experimentalists (Cline *et al* 1991). In order to make a

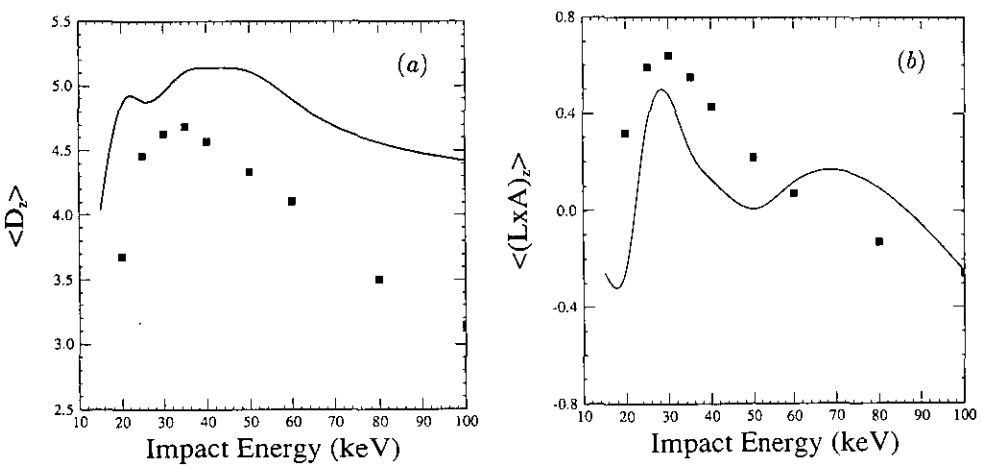


**Figure 2.** ($a$) Electric dipole moment $\langle D_z\rangle$ for $H^+ + He(1s^2) \rightarrow H(n=3) + He^+$. Theory: ——, present results. Experiment: ■, Ashburn *et al* (1990). ($b$) Averaged $\langle(\boldsymbol{L}\times\boldsymbol{A})_z\rangle$, symbols as in ($a$).

comparison between the calculated and the experimental elements of the density matrices we first compare our calculated cross sections for capture to the 3s state with the experimental data of Ashburn *et al* (1990) and of Brower and Pipkin (1989) in figure 3. Though agreement in general is good, yet the predicted values are lower than the experimental data near the cross section maximum and lie between the two experimental values at higher energies. One can expect similar errors to be reflected in the normalized (to 3s) elements of the density matrices considered next. We further note that the results for the 3d manifold should be taken with caution for the highest energy considered, as some numerical inaccuracies in the calculation were observed.

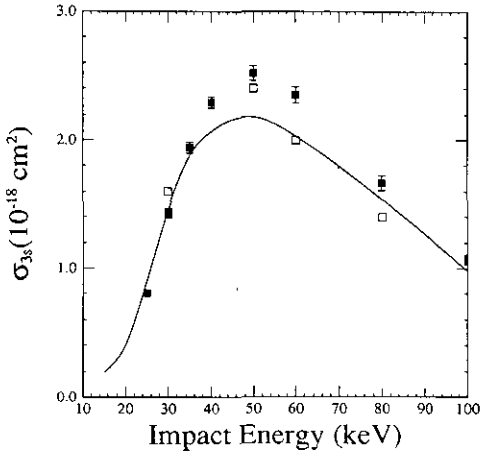


**Figure 3.** Electron capture cross section for $H^+ + He(1s^2) \rightarrow H(n = 3s) + He^+$. Theory: ——, present results. Experiment: ■, Ashburn *et al* (1990); □, Brower and Pipkin (1989).

The present normalized $3p_0$ and $3p_1$ cross sections are compared with the experimental data of Ashburn *et al* (1990) and Brower and Pipkin (1989) in figures 4(*a*) and (*b*) , respectively. For $3p_0$, the calculation agrees with both sets of data quite well. One notes that capture to $3p_0$ is much less than capture to 3s at energies above 30 keV. The normalized $3p_1$ cross section is in good agreement with experiments only at lower energies. At higher impact energies the data from the two sets of experiments differ significantly, by almost a factor of ten above 50 keV. Our results are closer to those of Brower and Pipkin (1989). In figures 4(*c*)-(*e*), the predicted $3d_0$, $3d_1$ and $3d_2$ cross sections (relative to 3s) are compared with the experimental data of Ashburn *et al* (1990) and Brower and Pipkin (1989). A good agreement between the experimental and the calculated $d_0$ and $d_1$ cross sections is found. In contrast, the calculated cross section for the partial $d_2$ cross section is closer to the experimental result of Brower and Pipkin (1989) which in turn is lower than the experimental data of Ashburn *et al* (1990). It is noted that these cross sections are very small.

### *3.3. Off-diagonal density matrix elements*

We next compare the calculated and the experimental (Ashburn *et al* 1990) normalized off-diagonal density matrix elements in figures 5–8. For the real part of the $sp_0$ matrix

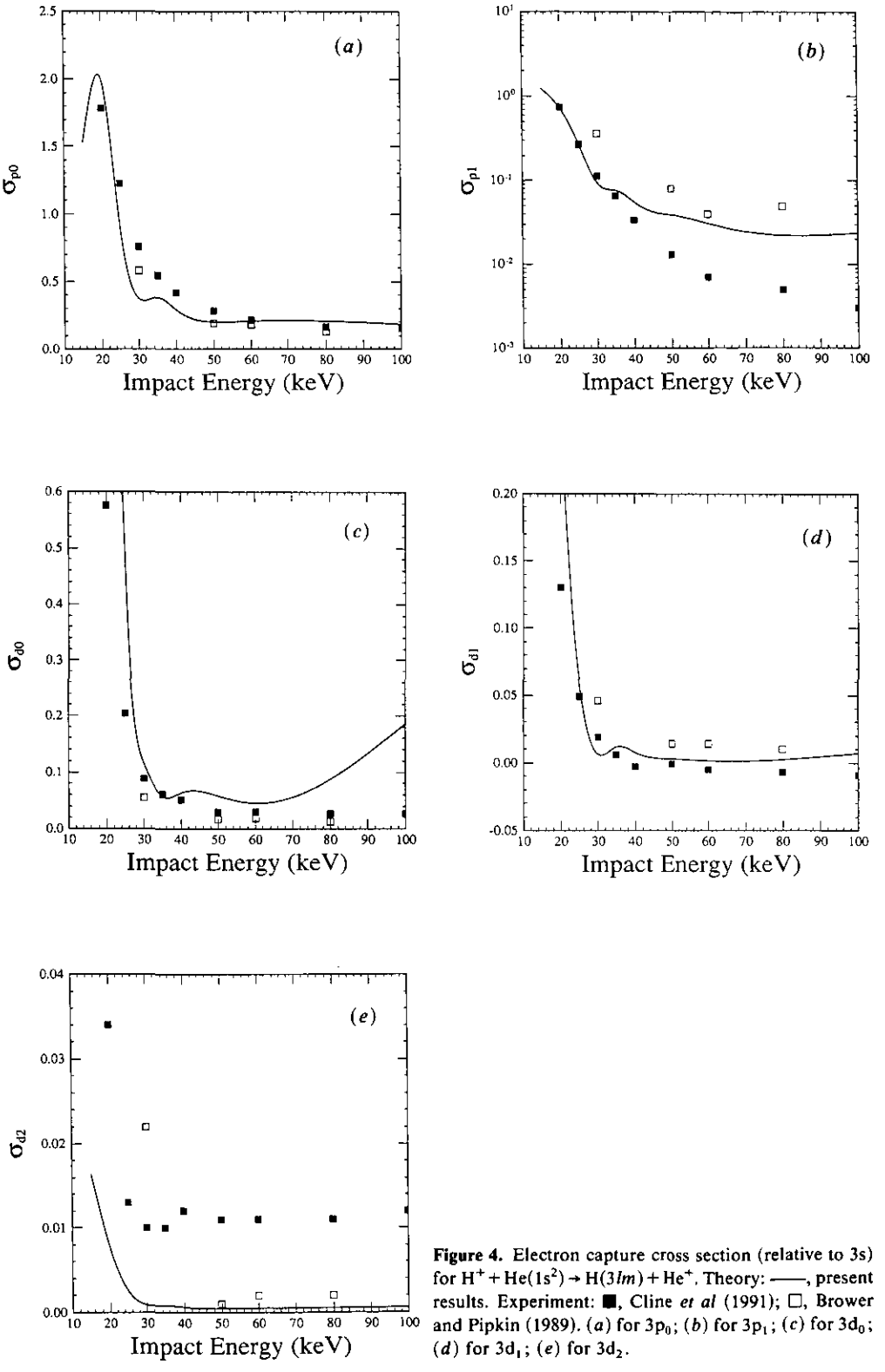


**Figure 4.** Electron capture cross section (relative to 3s) for $H^+ + He(1s^2) \rightarrow H(3lm) + He^+$. Theory: ——, present results. Experiment: ■, Cline *et al* (1991); □, Brower and Pipkin (1989). (*a*) for $3p_0$; (*b*) for $3p_1$; (*c*) for $3d_0$; (*d*) for $3d_1$; (*e*) for $3d_2$.

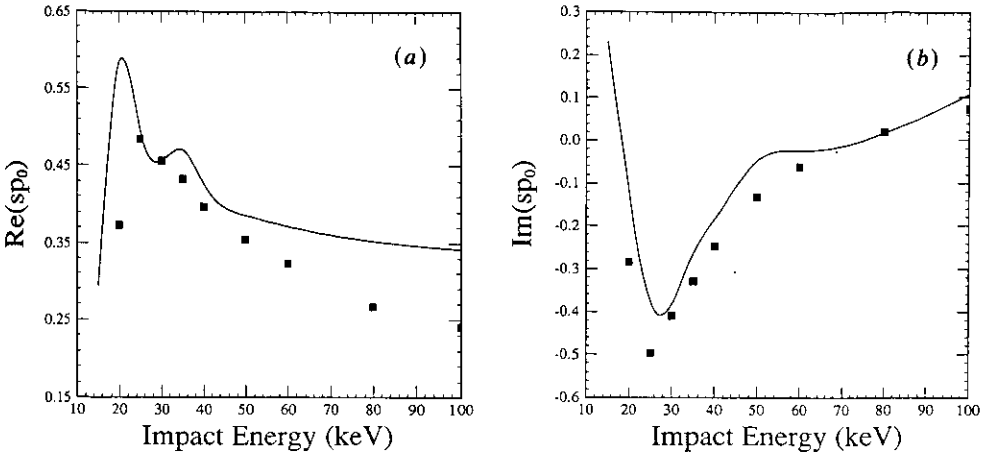


**Figure 5.** (*a*) Real and (*b*) imaginary part of the off-diagonal element $sp_0$ (relative to 3s) of the density matrix for $H^+ + He(1s^2) \rightarrow H(n=3) + He^+$. Theory: ——, present results. Experiment: ■, Ashburn *et al* (1990).

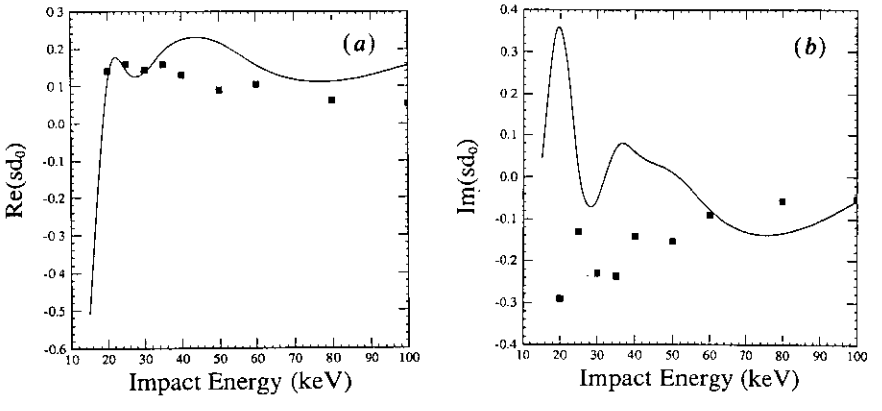


**Figure 6.** Same as figure 5 except for the $sd_0$ element.

element (figure 5(*a*)), the theoretical values are in good agreement with experimental ones except at higher energies where the latter are smaller. For the imaginary part the overall agreement is good over the entire range of energies (figure 5(*b*)). For the real part of the $sd_0$ matrix element, both the theoretical and experimental results (figure 6(*a*)) show very little energy dependence over the energy region under consideration. For the imaginary part, the experimental data show large scattering and the theoretical results also display strong energy dependence (figure 6(*b*)). One may state that there is no agreement at all for this matrix element between theory and experiment. The real part of $p_0d_0$, as shown in figure 7(*a*), shows that there is a general agreement between the theory and the experiment except for lower energies. Even the imaginary component (figure 7(*b*)) shows reasonable agreement between theory and experiment—unlike the discrepancy observed in figure 6(*b*) for the imaginary part of $sd_0$. Finally, the real and

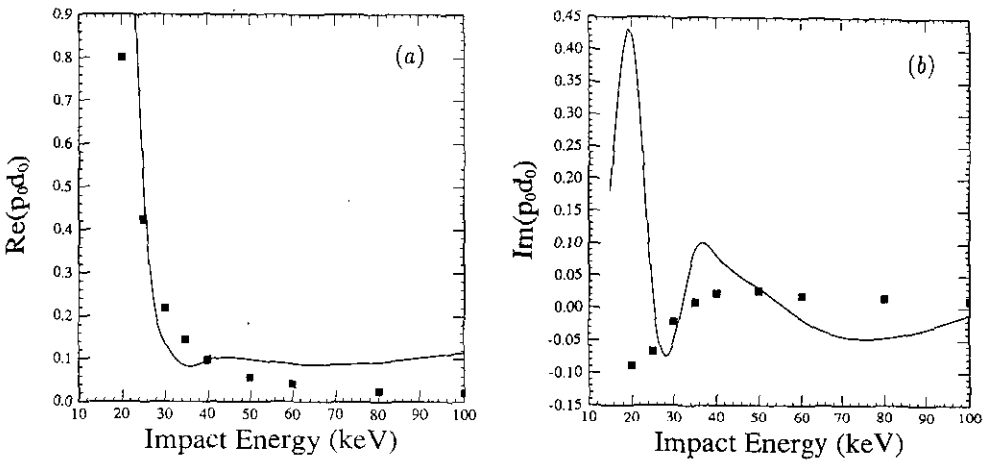


**Figure 7.** Same as figure 5 except for the $p_0d_0$ element.

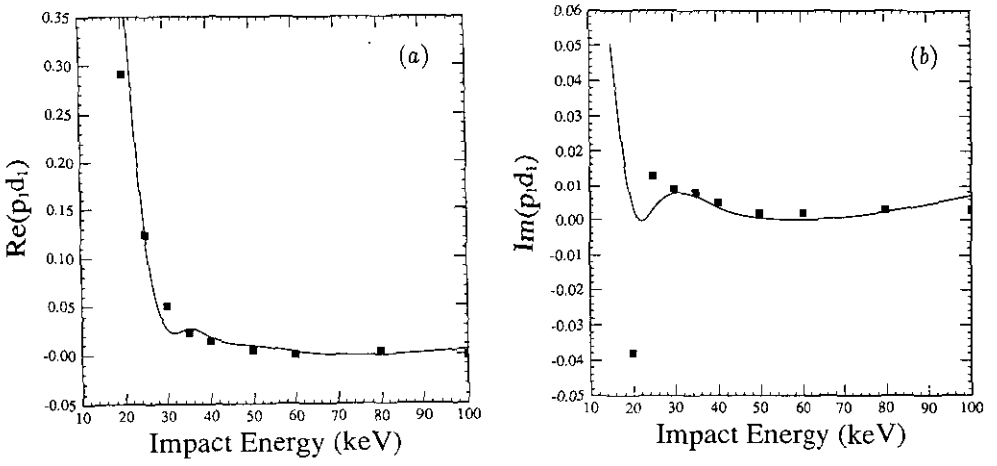


**Figure 8.** Same as figure 5 except for the $p_1d_1$ element.

imaginary components of the $p_1d_1$ density matrix element, as shown in figures 8(*a*) and (*b*), display surprisingly good agreement between the calculations and experiments in spite of the smallness of the magnitude for each component.

### *3.4. The alignment parameter $A_{20}$*

We next turn our attention to the integral alignment parameter $A_{20}$ for electron capture to 2p states in collisions of protons with helium atoms. Our calculated values and the experimental results of Hippler *et al* (1986) and of Teubner *et al* (1970) are shown in figure 9. The agreement between the calculated and the experimental values is reasonable for projectile energies between 15 and 55 keV. A test calculation was done at

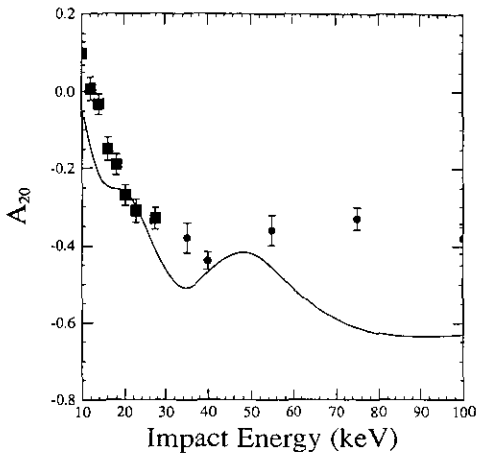


**Figure 9.** Integral alignment parameter $A_{20}$ for $H^+ + He(1s^2) \rightarrow H(2p) + He^+$. Theory: ——, present results. Experiment: ●, Hippler *et al* (1986); ■, Teubner *et al* (1970).

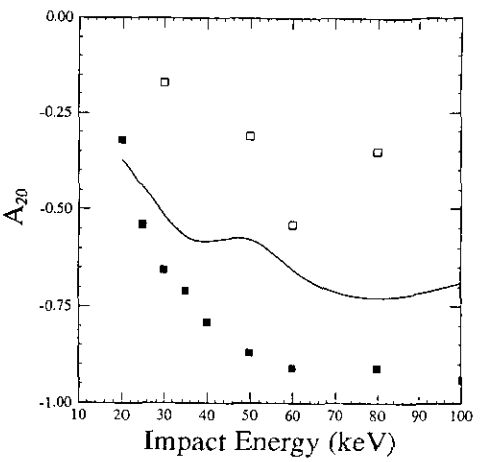


**Figure 10.** Integral alignment parameter $A_{20}$ for $H^+ + He(1s^2) \rightarrow H(3p) + He^+$. Theory: ——, present results. Experiment (see text): ■, Ashburn *et al* (1990); □, Brower and Pipkin (1989).

5 keV where the value of $A_{20}$ was found to be positive, in agreement with the experiment, indicating that the relative capture cross sections to $2p_0$ and $2p_1$ states can still be calculated by the present one-electron model. At higher projectile energies, the theory predicts a large negative value for $A_{20}$, indicating that the $2p_0$ state is populated predominantly, in contradiction to the small $A_{20}$ values from the experiment.

The integral alignment parameter $A_{20}$ for electron capture to the 3p state has not been measured directly. However, from the measured capture cross sections to $3p_0$ and $3p_1$ states of Ashburn *et al* (1990) and of Brower and Pipkin (1989), one can calculate the experimental values of $A_{20}$. The theoretical and experimental results are shown in figure 10. Because of the large difference in the $3p_1$ cross sections between the two experiments, the derived $A_{20}$ values are also quite different, with the theoretical values lying in between the two experimental results.

For collisions at higher energies, it is generally expected that the multipole moments constructed from each $n$-manifold scale simply with the principal quantum number $n$ (Burgdörfer 1986). For the alignment parameter $A_{20}$, the results for 2p and 3p states are expected to be identical (or at least nearly identical) at the higher energies, say, for energies greater than 60 keV. From figures 9 and 10, we note that the theoretical results are indeed quite close to each other, but this does not mean that the theoretical results are necessarily correct. The $A_{20}$ results of Brower and Pipkin (1990) for 3p are closer to the those of Hippler *et al* (1986) for 2p, but the data from the former show large scattering among the few energy points measured. The values of $A_{20}$ for the 3p state derived from the data of Ashburn *et al* (1990) are much more negative and decrease toward −1.0 at higher energies. This data set for the 3p state is not expected to coexist with the data of Hippler *et al* (1986) for the 2p state. Direct measurement of the alignment parameter for electron capture to the 3p state (i.e. measurement of the polarization of the Balmer-$\alpha$ radiation without an external electric field) is desirable.

## 4. Conclusions

In summary, the density matrices for the production of excited $n = 2$ and $n = 3$ hydrogen atoms in the passage of protons through the helium atoms have been calculated for 15–100 keV impact energies. The independent-particle model in conjunction with the multichannel semiclassical impact parameter approach and an expansion in travelling atomic orbitals placed on each scattering centre was used to calculate the scattering amplitudes. A basis set consisting of a large number of positive energy pseudostates was used to account for the ionization channels in the collision.

The calculated elements of the density matrix, the dipole moment, and the first moment of the electron current density for the $n = 3$ manifold of the hydrogen atom are compared with the recent measurements of Ashburn *et al* (1990). There is a general agreement between the calculated and experimental results for most of the elements of the density matrix over the energy range covered. However, there are still discrepancies in a few elements. In particular, the cross sections for capture to the $3p_1$ state display large discrepancies among the experiments and with theory. This is further reflected in the alignment parameter for the 3p state. It is suggested that a direct measurement of the alignment parameter for electron capture to the 3p state be carried out.

Experimental data exist for the $H(n = 2)$ density matrices at low energies ($<15$ keV) and for $H(n = 3)$ at higher energies ($>30$ keV). It is desirable that measurements for both sets can cover the whole energy range from say, 2–100 keV. By comparing the multipole moments between the two manifolds at the higher energies, one can further check the consistency of the different sets of experiments. The present theoretical model is not expected to work in general at lower energies, say, below 25 keV, where a description based on the two-electron description of the collison is essential. Such calculations can be carried out using the close-coupling method, with either molecular or atomic orbitals. A reasonable size of basis functions is adequate since in the lower energy region cross sections for single ionization are small. Experimental determination of the whole density matrix for capture to the $n = 2$ and $n = 3$ excited states over a wide energy range would provide the critical test needed to assess the various questions still in existence in ion–atom collision theories, such as the electron translational factors in the MO approaches, and the utility of united-atom orbitals in the AO approaches.

## Acknowledgments

This work is partially supported by the Division of Chemical Sciences, Office of the Basic Energy Sciences, US Department of Energy.

## References

Ashburn J R, Cline R A, van der Burgt P J M, Westerveld W B and Risley J S 1990 *Phys. Rev.* A **41** 2407
Blum K 1981 *Density Matrix Theory and Applications* (New York: Plenum)
Bransden B H, Ermolaev A M and Shingal R 1984 *J. Phys. B: At. Mol. Phys.* **17** 4515
Brower M C and Pipkin F M 1986 *Bull. Am. Phys. Soc.* **31** 994
—— 1989 *Phys. Rev.* A **39** 3323
Burgdörfer J 1983 *Z. Phys.* A **309** 285
—— 1986 *Phys. Rev.* A **33** 1578

Cline R A, Westerveld W B and Risley J S 1991 *Phys. Rev.* A to be published
DeSerio R, Gonzalez-Lepera C, Gibbons P, Burgdoerfer J and Sellin I A 1988 *Phys. Rev.* A **37** 4111
Eck T G 1973 *Phys. Rev. Lett.* **31** 270
Fano U and Macek J H 1973 *Rev. Mod. Phys.* **45** 553
Fritsch W and Lin C D 1986 *J. Phys. B: At. Mol. Phys.* **19** 2683
Havener C C, Rouze N, Westerveld W B and Risley J S 1986 *Phys. Rev.* A **33** 276
Hippler R 1990 Private communication
Hippler R, Harbich W, Faust M, Lutz H O and Dube L J 1986 *J. Phys. B: At. Mol. Phys.* **19** 1507
Jain A, Lin C D and Fritsch W 1987a *Phys. Rev.* A **35** 3180
—— 1987b *Phys. Rev.* A **36** 2041
—— 1988 *Phys. Rev.* A **37** 3611(E)
Krotkov R 1975 *Phys. Rev.* A **12** 1793
Sellin I A, Mowat J R, Peterson R S, Griffin P M, Laubert R and Haselton H H 1973 *Phys. Rev. Lett.* **31** 1335
Shingal R 1988 *J. Phys. B: At. Mol. Opt. Phys.* **21** 2065
Shingal R and Bransden B H 1989 *Nucl. Instrum. Methods* B **40/41** 242
Shingal R, Bransden B H and Flower D R 1989 *J. Phys. B: At. Mol. Opt. Phys.* **22** 855
Teubner P J O, Kauppila W E, Fite W L and Girnius R J 1970 *Phys. Rev.* A **2** 1763